

Chapter 3

Results and Discussion

3.1 Result and Discussion

In the electrochemical method there are two fundamental factors which have substantial effects on the quantity and quality of the SWGSs. Firstly, concentration of the electrolyte and secondly, amount of the applied potential.

As we explained in the introduction section about the role of electrolyte concentration in the intercalation and exfoliation phenomena and by considering explanations in the appendix A, 0.1M SDS solution is a good choice to use as the electrolyte [79, 67].

In order to have an exact study on this system, we focused only on one variation; applied potential. Since, SDS molecules in water will be ionized, by applying voltage DS^- will be adsorbed on the anode surface (graphite) Fig. 3.1.

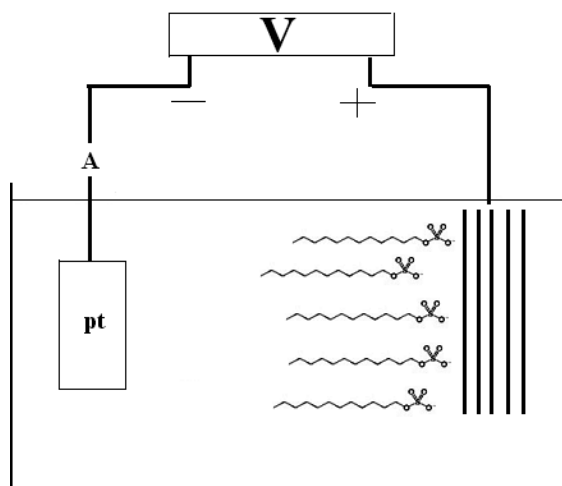


Fig. 3.1 Schematic scheme of intercalation process.

The reaction between graphite (C_x) and DS^- in the solvent (y) can be presented as [79]:



During this reaction, DS^- anions perch among the graphite layers via the formation of π - π chemical bonds with the layers surface which results in the intercalation of graphite [66]. On the other hand, the carbonic chains of DS^- are responsible for the exfoliation of graphite layers. Fig. 3.2 shows a schematic of intercalation and exfoliation of graphite layers.

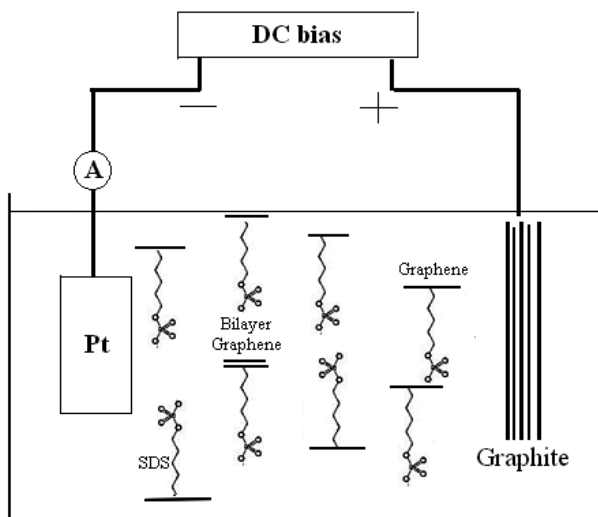


Fig. 3.2 Schematic illustration of the electrochemical and exfoliation of graphite layers to produce SWGSs suspension.

It should be also pointed out again that SDS is an amphiphilic surfactant (with hydrophobic and hydrophilic sections) which results in the stability of prepared SWGSs in the aqueous media.

3.2 Characterization of SWGSs

3.2.1 Chronoamperometry

The transfer of DS^- between graphite layers is a diffusion controlled phenomenon. The CTT curves obtained at different applied potentials (Fig. 3.3) indicates that at initial time of process, the concentration of DS^- at the interface of electrolyte/electrode is high enough and consequently, the diffusion of DS^- into graphite layers is a rapid step (Fick's second law).

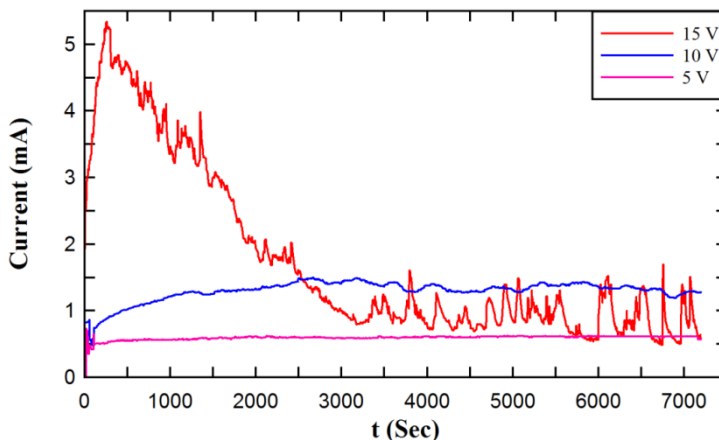


Fig. 3.3 The CCT curves obtained at different potentials in the SWGSs producing.

However, after this initial time, the current drop is inevitable due to an increase in the resistance of electrolyte (limited diffusion). Close observation of Fig. 3.3 shows that at applied potential of 15 V, the efficiency of intercalation step increases as a result of higher electrical driving force; the higher electrical driving force leads to a higher stress applied over the anode compared to other potentials. Regarding the higher rate of solute diffusion at 15 V applied potential, the production yield of high quality SWGSs increases. Under saturation conditions,

the graphite surface is covered by a thin film of SDS which acts as a capacitor; this hinders the diffusion of DS^- and consequently, all CTT curves approach to a constant value after a period (Fig. 3.3). Moreover, the significant fluctuations observed in the CTT curve corresponding to 15 V can be attributed to higher electrical driving force; i.e. the high driving force leads to repetitive exfoliation of SWGSs over the graphite surface and results in the formation of fresh surface during the electrochemical process [100, 94].

Another evidence for the repetitive exfoliation of SWGSs is the color of graphene/SDS suspension prepared at different applied potentials; the higher level of applied potential results in the darker color of samples (Fig. 3.4) which can be attributed to higher level of exfoliated graphite present in the solution [100, 66].



Fig. 3.4 Image of the prepared samples in different applied potentials.

The estimated amounts of SWGSs are 11.3, 7.65 and 5 g/L for 15, 10 and 5 V potentials, respectively; these results are in good agreement with chronoamperometry analysis.

3.2.2 Raman Spectroscopy

Fig. 3.5 shows the Raman spectra of SWGSs obtained at different applied potentials.

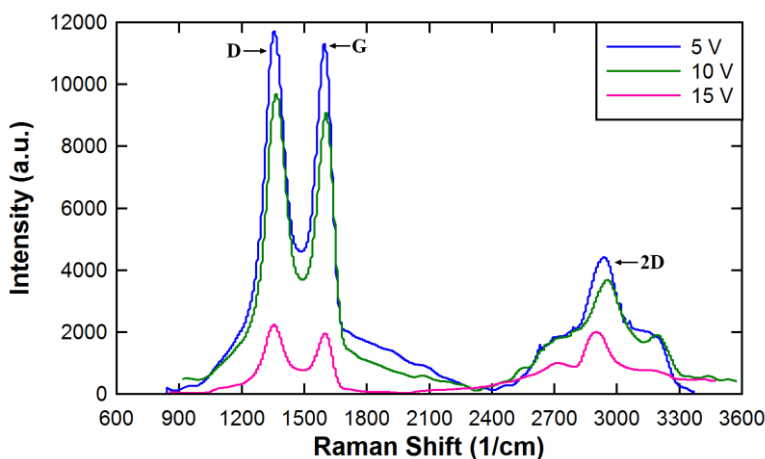


Fig. 3.5 Raman spectra of the obtained SWGSs in different applied potentials.

The presence of D, 2D and G peaks [95] in all spectra confirms the formation of SWGSs in all conditions. Regarding the fact that the lower number of graphene layers results in narrower 2D peak with red shifts [94], it can be concluded that an increase in the level of applied potential leads to the formation of lower number of graphene layers [96]. However, the shape and frequency of 2D peak are affected by the layer numbers of GSs [95, 34]. The 2D band of the monolayer GSs appears at 2679 cm^{-1} , while the 2D peak of 2-4 layers shifts to 2798 cm^{-1} ($+19\text{ cm}^{-1}$) [95]. Regarding the Raman spectra presented in Fig. 3.5, the appearance of 2D peak at 2698 cm^{-1} confirms the formation of 2-4 layers SWGSs. However, since 2D peak in the spectrum corresponding to 15 V is neither sharp nor symmetric, it is most likely that a mixture of monolayer and multilayer SWGSs has been obtained under these

conditions. Another important point regarding graphene layer thickness is the intensity of G band [96]. It is worthy of note that the peak corresponding to the G band of the single layer of graphene occurs at $\sim 1585 \text{ cm}^{-1}$ and the shift in the position of the G band $\sim -6 \text{ cm}^{-1}$, is due to the stacking 2-6 layers [97]. According to the Fig. 3.5 the observed peak at $\sim 1580 \text{ cm}^{-1}$ can be also assigned to the presence of a mixture of monolayers and multilayer SWGSs. Close observation of Fig. 3.5 reveals that the SWGSs obtained at 15 V have minimum number of the layers.

The defects percentage of the obtained SWGSs at different applied potentials can be estimated using [98, 99]:

$$X_G = \frac{I_G}{I_G + I_D}, X_D = 1 - X_G \quad \text{Eq. 3.2}$$

Where X_G and X_D are the molar fraction of carbon atoms with regular and irregular SP^2 bond, respectively. Also, I_G and I_D are the intensity of G and D peaks appeared in Raman spectrum. The results of this exercise indicates that the amount of carbon with regular SP^2 bond slightly decreases by increasing applied potentials which is due to the more interactions between GSs and SDS molecules and partial oxidation of the SWGSs at the higher applied potential. Also, the broadness of the peaks observed in the Raman spectra (Fig. 3.5) indicates the presence of highly functionalized SWGSs due to the strong interactions between SDS molecules and GSs [100].

3.2.3 FT-IR Analysis

FT-IR spectrum of the SWGSs produced at 15 V has been shown in Fig. 3.6. It is worthy of note that in this FT-IR spectrum, prominent features corresponding to graphene oxide, including absorption bands corresponding to C–O stretching at

1053 cm^{-1} , phenolic O–H deformation vibration at 1412 cm^{-1} , C = C ring stretching at 1621 cm^{-1} , C=O carbonyl stretching at 1733 cm^{-1} , are not present [101]. However, the characteristic stretching bands at 3485 and 1224 cm^{-1} corresponding to OH and C-OH [102] indicate partial oxidation of the SWGSs during exfoliation/dispersion step [68]. Also, the stretching bands of the C-H functional groups as well as the C-H vibration band appear at 2920 , 2850 and at 1470 cm^{-1} , respectively [66].

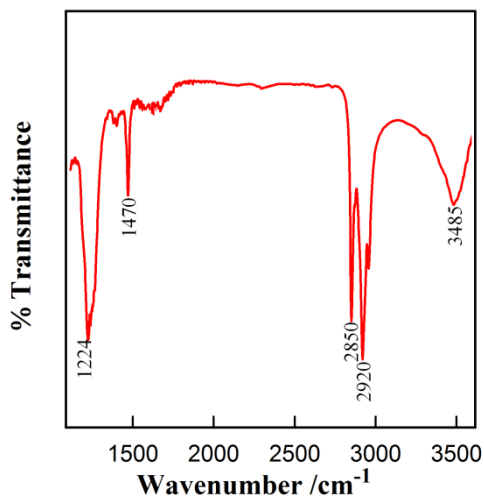


Fig. 3.6 FT-IR spectra of SWGSs produced at 15 V.

3.2.4 AFM Result

According to the AFM image presented in Fig. 3.7, the thickness of the thinnest SWGSs obtained at 15 V is estimated around 1.87 nm.

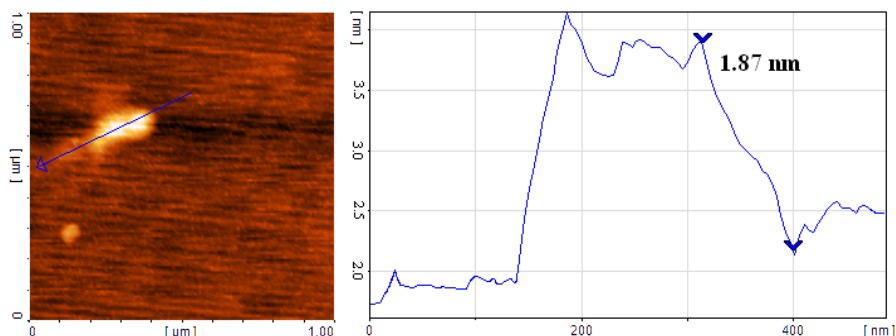


Fig. 3.7 AFM image of prepared SWGSs in applied 15V.

Regarding the thickness of pristine GS (~ 0.34 nm), it can be concluded that SWGSs consist of 1–3 layers of GS [34]. It should be pointed out that the presence of solvent/SDS molecules, oxidized parts and functionalized groups in the SWGS as well as crumpling and scrolling of the SWGS due to thermal fluctuations can result in the overestimation of thickness via AFM [66]. The circular shape of the obtained SWGSs (Fig. 3.7), which appears as a result of solution treatment and formation of nanoparticles colloid, is due to achieving minimum surface area. On the other hand, high speed centrifugation results in the agglomeration of some SWGSs [79].

3.2.5 X-Ray Diffraction

In Fig. 3.8, the XRD patterns corresponding to the graphite and electrochemically synthesized graphene at 15 V are presented.

As it can be observed, a high percentage of graphite layers have been converted to SWGSs after the synthesis process; the sharp peak at $2\theta = 26$ related to (002) graphite disappears in the XRD pattern of graphene. Moreover, the peak broadening from $2\theta = 12.7$ to 40 indicates the presence of different number of graphene layers [79, 103].

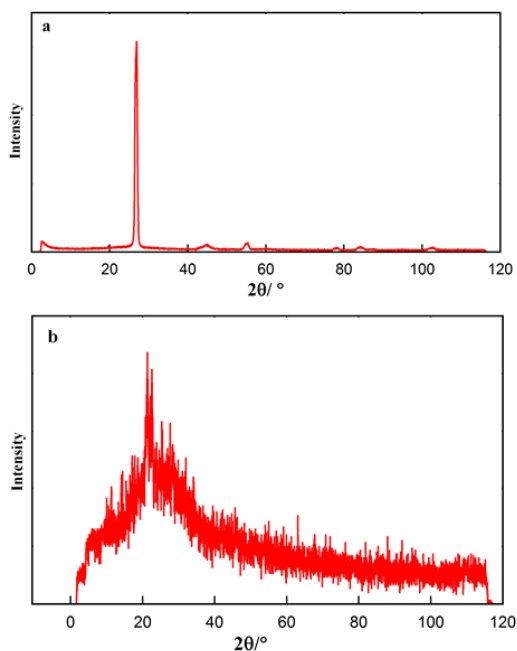


Fig. 3.8 XRD patterns of (a) raw graphite and (b) SWGSs produced at 15 V.

3.2.6 Electron Microscopic Studies

Fig. 3.9 shows the FESEM images of SWGSs obtained at 15 V. It is worthy of note that the majority of waves observed in graphene sheet structure are transparent (Fig. 3.9 a). Also, the buckling/wrinkling appeared in some SWGSs is due to thermodynamic stability of 2D structure of graphene [34].

The transparency and thickness of multilayers SWGSs were evaluated using TEM. Fig. 3.10 shows both the monolayer and multilayers SWGSs (black arrays).

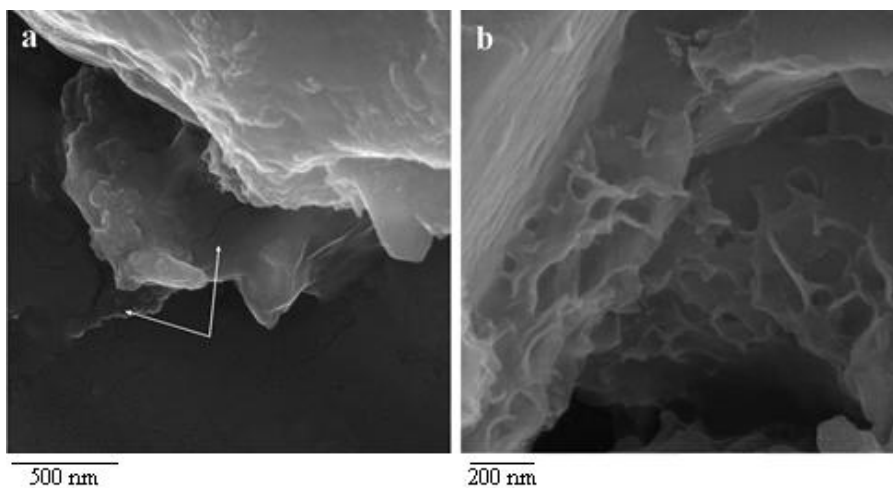


Fig. 3.9 FESEM images of the synthesized SWGSs at 15 V.

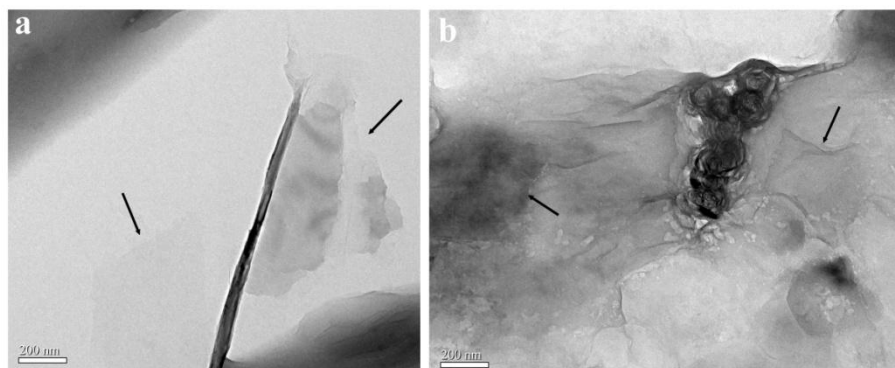


Fig. 3.10 TEM images of the synthesized SWGSs at 15 V.

Additionally, the interlayer distance of SWGSs is estimated around 0.34 nm based on HRTEM observation (Fig. 3.11), which is in agreement with the bilayer distance of graphite planes [113].

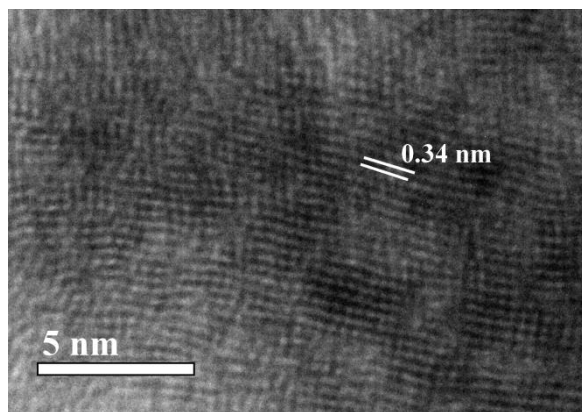


Fig. 3.11 HRTEM image of the interlayer distance in synthesized SWGSs at 15 V.

Also, the synergistic combination of the high specific surface area and strong nano-filler-matrix adhesion as well as the exceptional mechanical properties of the sp^2 carbon network in GSs [91] improves the mechanical properties of polymer nanocomposites [82, 84]. On the other hand, the electrochemical production of SWGSs in the presence of a surfactant is known as one of the facile and controllable method for the fabrication of high quality GSs in a large scale.

3.3 Characterization of SWGSs/PVA Nanocomposite Films

3.3.1 XRD Patterns

In order to assess the structure, crystallinity percentage and interlayer changes of the fabricated nanocomposites, XRD was carried out. The sharp peak around $2\theta=19.4$ (d-spacing of 0.45 nm) and the feeble bulge appeared at $2\theta=40.4$ (d-spacing of 0.22 nm) (Fig. 3.12) are assigned to the semi-partial crystalline structure of PVA [68]. Also, the disappearance of the broad peak

corresponding to SWGSs is contributed to molecular level dispersion of SWGSs in PVA matrix resulted in loss of structure regularity of SWGSs [86]. As can be observed, the (101) peak is intensified at the higher level of SWGSs in the polymer matrix which is contributed to an increase in the number of PVA chains packing. In fact, the SWGSs act as the nucleating agents and accordingly, the crystallinity of the composites improves.

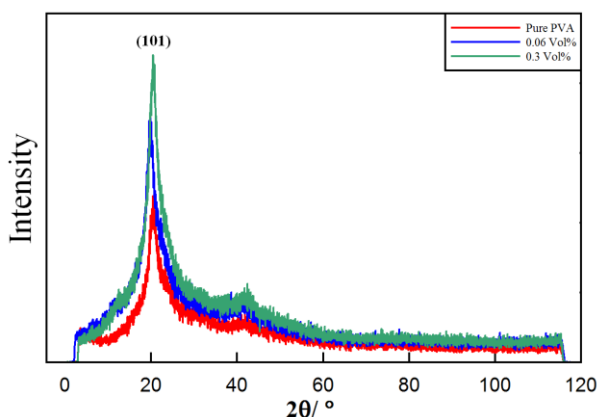


Fig. 3.12 XRD patterns of SWGSs/PVA nanocomposit with various graphene contents.

3.3.2 Mechanical Properties

As it has been mentioned previously, to have maximum composite modulus the relation between number of GSs for reinforcing polymers and the polymer layer thickness should be taken in account. Thus, about the PVA [104] multi-layer SWGSs can obtain the maximal mechanical properties of the nanocomposites. In Fig. 3.13 the column curves of the mechanical properties of the prepared composite films at 45 and 60 °C with various SWGSs loading are presented.

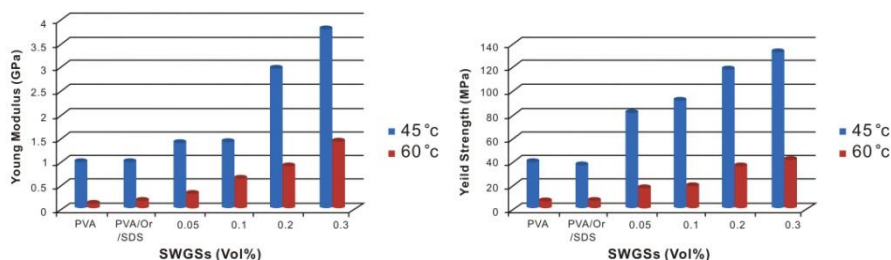


Fig. 3.13 Comparison between mechanical properties of the prepared samples at 45 and 60 °C.

As it can be observed, the strength and young's modulus of the nanocomposites increase by increasing the percentage of the SWGSs. The physicochemical interactions between the pendant hydroxyl groups of PVA with SDS molecules accompanied by GSs (hydrogen bonding) [105], result in improvement of the nanocomposite films' mechanical properties even at low loading SWGSs.

According to Fig. 3.14, the nanocomposites reach a mechanical percolation point (0.2 and 0.1 Vol% SWGSs for the nanocomposites prepared at 45 and 60 °C, respectively).

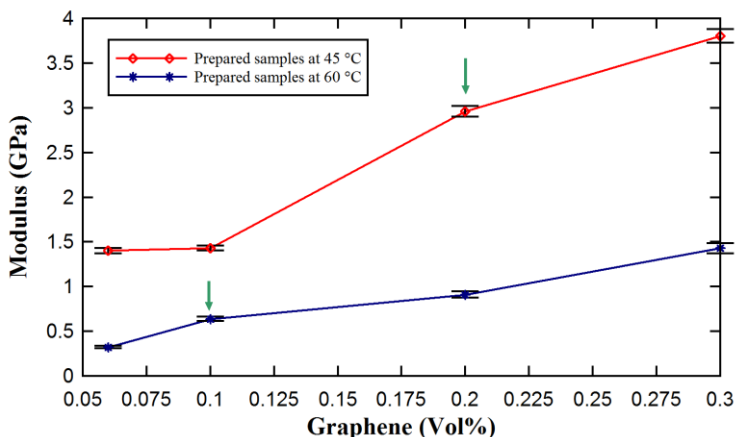


Fig. 3.14 Young's modulus of the nanocomposite films versus SWGSs loadings.

At the percolation point, there is a long-range interaction between random chains of PVA and SWGSs. In fact at this point, the chains of the PVA and SWGSs form a 3D structure and consequently, the chains of polymer cannot move easily [86]; i.e. the mechanical properties of the nanocomposites are enhanced. The main and distinctive point between the obtained results with previous works [82, 91, 86, 105, 106, 107] is the low level of SWGSs used for the fabrication of the nanocomposites; i.e. the uniform distribution of the reinforcements in polymer matrix [107, 86] is achieved by adding only 0.2 and 0.1 Vol % SWGSs in the nanocomposites prepared at 45 and 60 °C.

It is remarkable that the prepared nanocomposite films at 45 °C show yielding points in their stress-strain curve, while, the produced films at 60 °C do not have yielding point and their strength increase uniformly till fracture point (Fig. 3.15).

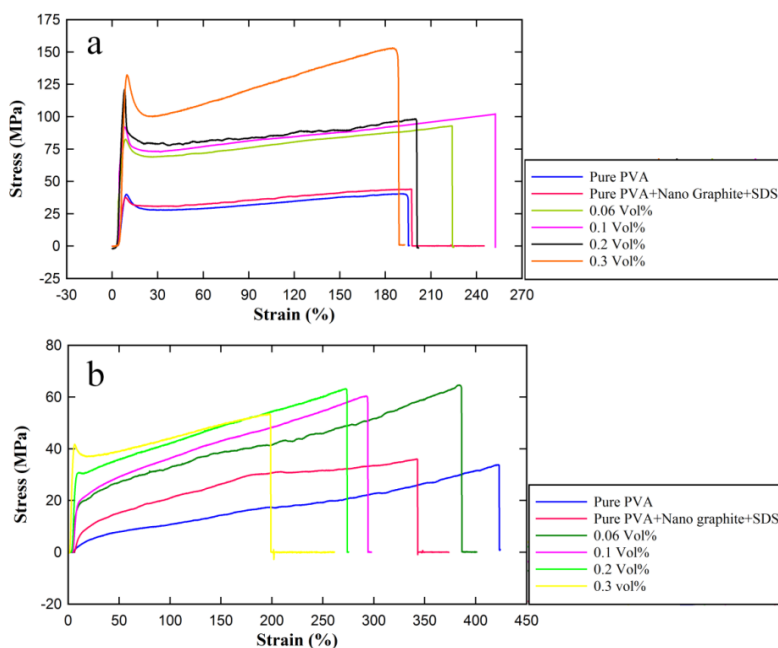


Fig. 3.15 The stress-strain curves of SWGSs/PVA nanocomposite films (a) at 45 °C and (b) 60 °C.

3.3.3 Thermal Studies

In order to study the effect of SWGSs on the dynamic crystallization of PVA and the macroscopic properties of the nanocomposite films, DSC was conducted. As it is shown in table 3.1, the T_p gradually increases by increasing the graphene loading level; this reveals that the SWGSs act as seeds for the faster nucleation (confirmation the XRD results in 3.3.1 sec.) [108].

Table 3.1 *The percent of crystallinity and T_p of the nanocomposite films.*

| Samples | Crystallinity (%) | T_p |
|-------------------|-------------------|-------|
| Pure PVA at 45°C | 17.2 | 191.2 |
| Pure PVA at 60°C | 16.07 | 188.4 |
| 0.2 % Vol at 45°C | 20.2 | 193.1 |
| 0.1% Vol at 60°C | 25.24 | 194.7 |

The crystallinity of PVA and the nanocomposites can be calculated by using of the DSC analyze (the enthalpy of 100% crystallinity of PVA is 138.6 J/g [109, 110]). By considering the weight fraction of PVA in the nanocomposite films, the crystallinity of PVA is determined.

Thus, the significant improvement in the mechanical properties of the nanocomposites stems from the presence of these crystalline shells which creates an effective attachment of PVA to the nanosheets of SWGSs that constrains the segmental motion of the polymer chains [105].

According to the results given in table 3.1, in the presence of SWGSs, the variation in the crystallinity percentages of the samples prepared at 60 °C is higher than that of at 45 °C; thus, the higher number of crystals at 60 °C results in the stacking the polymeric chains and accordingly, the elongation percentage reduces at higher level of reinforcement [108]. On the other hand, for the samples prepared at 45 °C, SDS molecules play the role a plasticizer.

It should be noted that the drying process of the nanocomposites was conducted from ambient temperature up to 45 and 60 °C. At the higher temperature range (ambient temperature to 60 °C), the movement of polymer chains is more than other sample; i.e. the structural order becomes lower at the higher temperature. Since, the time of drying process was set the same for both nanocomposite films, it can be concluded that the crystallinity percentage of samples that were dried in the range of ambient temperature to 45 °C, is higher.

An interesting point regarding the mechanical properties is that the percolation point corresponding to the sample prepared at lower temperature range (ambient temperature to 45 °C) occurs at 0.2 Vol % of SWGSs; while, for sample dried at higher temperature range, the percolation point is at 0.1 Vol % of SWGSs. The higher volume percentage of the SWGSs in the former case is another reason for the more crystallinity percentage of these samples.

For further evaluation, the TGA curves corresponding to the pure PVA films [84, 111, 112] are presented in Fig. 3.16.

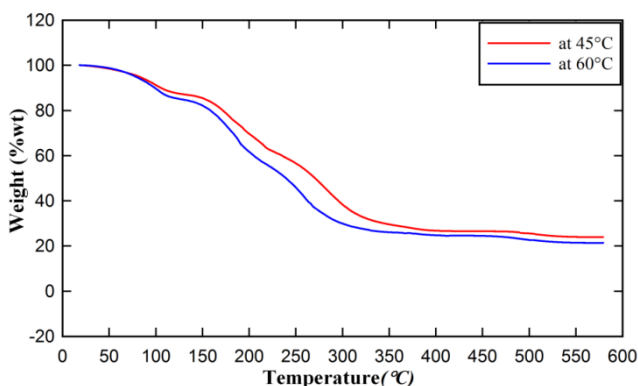


Fig. 3.16 TGA curves of the pure PVA films at 45 and 60 °C.

As it can be seen, the percentage of weight loss and decomposition rate for the sample prepared at 60 °C is higher than the sample prepared at 45 °C. Thus,

mobility of the SDS and polymer chains is higher in prepared samples at 60 °C and accordingly, there is less grafting between chains compared to the prepared films at 45 °C; so, a higher elongation and lower strength is observed in the case of nanocomposite prepared at 60 °C compared to that at 45 °C.

A comparison between the thermal and the mechanical properties of the pure PVA and SWGSs/PVA nanocomposites at the percolation threshold indicates that the SWGSs can effectively reduce the effect of degradation of the PVA during the synthesis process of nanocomposites (synergetic effect). Consequently, the yielding point of the nanocomposites shifts to the higher percentages of SWGSs for the prepared samples at 60 °C.

3.3.4 FE-SEM Studies

According to the FE-SEM images of the fracture surface of the nanocomposite films (Fig. 3.17) at their percolation points, layered-structures with fully exfoliated and well-dispersed SWGSs in the PVA matrix with the lowest amount of restacking the nanosheets compared to the pure PVA were revealed [105]. Furthermore, the images show that the SWGSs are distributed in a 3D network in the polymer matrix [86].

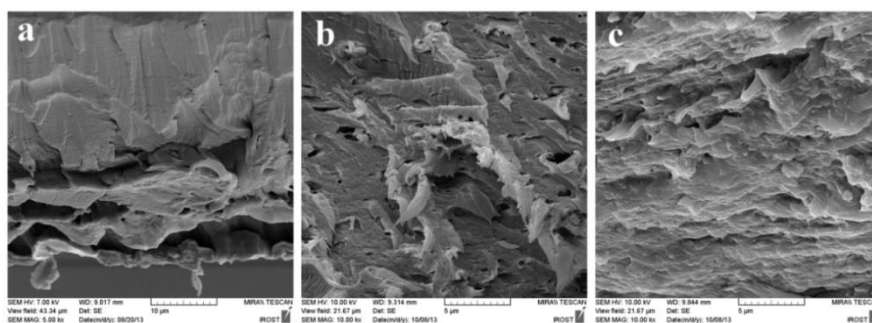


Fig. 3.17 The FE-SEM images of the (a) pure PVA, nanocomposite films prepared at (b) 45 °C with 0.2 Vol% SWGSs, and (c) 60 °C with 0.1 Vol %.

